MRS Communications

https://doi.org/10.1557/s43579-024-00547-2

MRS Communications

Advanced Catalytic Materials: Nano and Bulk Research Letter

Platinum nanoparticle synthesis in engineered organic nanoscale reactors for efficient oxygen electro-reduction in alkaline conditions

Subhajit Bhunia, Suzatra Chatterjee, and **Carlos R. Cabrera**, Department of Chemistry and Biochemistry, The University of Texas at El Paso, El Paso, TX 79968, USA

Address all correspondence to Carlos R. Cabrera at **crcabrerama@utep.edu**

(Received 17 November 2023; accepted 12 March 2024)

Abstract

We have designed a polymer, hc-TBtd-COP incorporating a Wurster-type redox-active building unit for the *in situ* reduction and nucleation of platinum nanoparticles which forms an organic polymer-wrapped metal nanoparticle composite. This composite exhibits exceptional mass activity (MA) (about 5 times larger than 20% Pt/C at 0.9 V vs. RHE) and specific activity (SA) (approximately 2 times larger than 20% Pt/C at 0.9 V vs. RHE) for the oxygen reduction reaction. The efficient electrocatalysis results from higher catalytic site dispersion and superior atom utilization efficiency. This research contributes to the advancement of composite materials for enhanced electrocatalytic performance.

Introduction

The oxygen reduction reaction (ORR) is a pivotal process in regenerative energy conversion, serving as a cornerstone in advanced technologies, like polymer electrolyte membrane fuel cells (PEMFCs) and metal-air batteries. Notably, proton exchange membrane fuel cells (PEMFCs) have garnered substantial attention for their ability to direct electrochemical conversion, largely attributed to the utilization of highly efficient ORR electrocatalysts. Among these, noble metals, particularly ultrafine-sized platinum (Pt) and Pt-based electrocatalysts, have shown promise.[1–3] Their smaller particle sizes provide larger surface areas with numerous defects, significantly enhancing catalytic activity for ORR. High Pt loading remains a cost challenge, and issues such as agglomeration of Pt NPs and corrosion of global support cease their long-term operational durability. Researchers have reported various NPs stabilizers, including surfactants, polymers, dendrimers, and ligands, as capping agents on carbon materials to mitigate these issues. However, the presence of these capping functionalities masking around the NPs may compromise their activity, necessitating the finding of alternative support functionality that can prevent active site aggregation without sacrificing catalytic performance. Despite making significant progress in achieving remarkable fuel cell efficiency using nanoparticles of Pt and Palladium (Pd) nanoparticle (NP) supported on conductive carbon materials with a higher surface area, concerns remain regarding their economic viability and durability.

Covalent organic frameworks (COFs) and polymers (COPs) have gained popularity as a reliable choice for stabilizing nanoparticles due to their stability and functional tenability.[4–8] COPs are hydrolytically stable organic polymers, making them excellent scaffolds for anchoring catalytic metal nanoparticles. Moreover, the incorporation of heteroatoms, such as nitrogen (N), and sulfur (S), into the COP frameworks endows covalent organic polymer/frameworks (COFs) with additional advantages as ideal supports for immobilizing active sites for catalysis.[9–11] Metal coordination sites have been incorporated into various functional COPs, allowing for the controlled nucleation of metal nanoparticles with a homogeneous size distribution within the COP structure. These resulting metal nanoparticle-supported COP systems (NP@COP) exhibit greatly improved electrochemical activity and long-term durability in electrocatalysis. However, there are two primary obstacles that COPs must overcome to become optimal scaffolds for noble metal-based electrocatalysis. Firstly, during the NPs immobilization process inside COPs, the reduction of metal ions by external reducing agents often leads to uncontrolled reduction.[12,13] This results in the growth of larger nanoparticles which leads to a lower exposure of active sites, which affects the atom utilization of precious metals.[14,15] Achieving selective reduction of metal ions within the pores of COPs remains a significant challenge. The second bottleneck in achieving a higher current-to-metal loading ratio from NP@COP is the inherently poorer conductivity of most COPs compared to conventional electrocatalyst materials, like carbon. As a result, the electrochemical activity of most NP@COP systems is significantly lower due to the charge-transfer limitations which can be attributed to the lower conductivity of the COPs matrix during the catalytic process. To date, most synthetic strategies for COP-supported electrocatalysts require pyrolytic treatment at higher temperatures to achieve improved conductivity, which may cause unwanted structural changes and undesired metal losses.[16] The development of highly efficient ORR electrocatalysts is crucial for the

Subhajit Bhunia and Suzatra Chatterjee have contributed equally to this work.

advancement of regenerative energy conversion technologies. While noble metals like Pt have shown promise, challenges remain, including reducing Pt loading with improved current density and improving long-term stability. COPs represent an exciting avenue for addressing these challenges, offering stability and versatile coordination sites. However, selective reduction and enhancing their conductivity remain key challenges in harnessing the full potential of COPs as electrocatalyst supports. As research continues in this field, the quest for a non-pyrolytic approach for noble metal-based electrocatalysts with defect-free structures and predictable active sites promises to be an exciting and essential area of investigation.

Material and methods

Catalyst synthesis

All chemicals and solvents were used as received without any further purification. Ultrapure water (Millipore Milli-Q grade) with a resistivity of 18.2 MΩ was used in all experiments. 2,1,3-Benzothiadiazole-4,7-bis (boronic acid pinacol ester) was purchased from Ambeed, Inc., USA. 4-Bromotriphenylamine, Potassium tetrachloroplatinate, Tetrakis (triphenylphosphine) palladium(0), and all the organic solvents are purchased from Millipore Sigma, USA. Anhydrous Potassium carbonate, HCl, and H_2SO_4 were purchased from Fisher Scientific, USA. Oxygen (O_2, 99.999%) and argon (Ar, 99.9999%) were supplied by Airgas, Texas.

Synthesis of 4,4′-(benzo[c][1,2,5]thiadiazole-4,7-diyl) bis(N,N-diphenylaniline) (TBtd)

To synthesize (TBtd), 2,1,3-Benzothiadiazole-4,7-bis (boronic acid pinacol ester) weighing 0.194 g (0.5 mmol), 4-Bromotriphenylamine weighing 0.33 g (1.01 mmol), K_2CO_3 (2 M, 1.5 mL) and $Pd(PPh_3)_4$ (57 mg; 0.05 mmol) were dissolved in 6 mL of Argon-saturated dioxane. Then, the mixture was then stirred at refluxing conditions for 30 h. After that, the reaction mixture was poured into ice water, and the organic layer was extracted using dichloromethane. The extracted solution was then dried over $MgSO_4$ and concentrated to dryness. The crude mixture was purified by column chromatography on silica with CH_2Cl_2/hexane = 2:3 as eluent to obtain the product as a pale yellow solid (202 mg, Yield = 64%). ^{1}H-NMR (600 MHz, $CDCl_3$) δ = 7.90 (d, J = 8.6 Hz, 4H), 7.77 (s, 2H), 7.31 (t, J = 8.0 Hz, 8H), 7.25–7.20 (m, 12H), and 7.09 (t, J = 7.3 Hz, 4H).

Synthesis of hc-TBtd-COP

A solution of TBtd (93 mg, 0.15 mmol) in 1,2-dichloroethane (6.0 mL) was transferred dropwise to a suspension of anhydrous $FeCl_3$ (250 mg, 1.56 mmol) in anhydrous 1,2-dichloroethane (5.0 mL). Then, the reaction mixture was heated to reflux for 8 h. After cooling down the reaction mixture, methanol (1 L) was poured into the mass and continuously stirred for 30 min. Then, the solid precipitate was filtered and washed with methanol, tetrahydrofuran, and water repeatedly to remove entrapped monomer and catalyst residues. The solid sample was extensively washed with tetrahydrofuran and methanol using a Soxhlet apparatus as solvents for 24 h. Finally, the solid material was dried under vacuum for 24 h at 50°C to isolate the polymer as reddish-brown powder (51 mg, 54% yield).

Synthesis of Pt@hc-TBtd-COP

In a standard synthesis procedure, 3 mg of K_2PtCl_4 was dissolved in a 5-ml water/ethanol mixture (1:1 v/v). Subsequently, 50 mg of hc-TBtd-COP was introduced into the solution, followed by 30 min of ultrasonication at room temperature to achieve a homogeneous solution. The resulting mixture was then transferred into a glass ampule and heated in an oven at 55°C for 6 h. The resulting blackish-brown precipitate was filtered and subjected to washing with ethanol and water to eliminate any unreacted platinum salt. Finally, the product was dried under a vacuum overnight.

Electrochemical measurements

Electrochemical measurements were conducted utilizing both alkaline (0.1-M KOH) and acidic (0.5-M H_2SO_4) electrolytes in a conventional three-electrode system on an electrochemical workstation (Pine). The setup included a Platinum (Pt) coil as the counter electrode, while Ag/AgCl (4-M KCl) served as a reference electrode, respectively. The working electrode was a rotating ring disk electrode (RRDE) with a disk diameter of 5 mm and a ring area of approximately 0.109 cm^2. Pt@hc-TBtd-COP/acetylene black (6 mg; 1:1) was dispersed in a 980-µL ethanol/water mixture (4:1) containing 5-wt% Nafion (20 µL). The resulting catalyst ink was sonicated for 2 h at room temperature to ensure a homogeneous dispersion. Subsequently, 5 µL of the ink was drop cast on the RRDE disk electrode area, forming a catalytic layer over the glassy carbon (GC) disk electrode and left to dry overnight. The loading density of all catalytic ink was maintained at approximately 0.15 mg cm^{-2}. GC area of RRDE serves as the primary working electrode and Pt ring serves as secondary working electrode. iR corrections were applied to all potential reported in this study. Potential values were calibrated and converted to the reversible hydrogen electrode (RHE) using the formula: E (vs. RHE) = E (vs. SCE) + 0.244 V + 0.059*pH-iR, in 0.1-M KOH and 0.5-M H_2SO_4. For the preparation of the working electrode, Oxygen reduction reaction (ORR) measurements were conducted using various electrochemical techniques, including linear sweep voltammetry (LSV), cyclic voltammetry (CV), and electrochemical impedance spectroscopy (EIS). CV curves were recorded within a potential range of 1.2 V to 0.2 V vs. RHE at a scan rate of 10 mV/s after the electrolyte was purged with oxygen (O_2) for at least 30 min. Before the experiment, 50 cycles of CV (50 mV/s) were recorded to activate the catalyst. LSV curves were measured in O_2-saturated 0.1-M KOH electrolytes and 0.5-M H_2SO_4 with the rotating speed ranging from 400 to 2000 rpm and a sweep rate of 10 mV/s. The current density was calculated from the current normalized by

the geometrical area of the GC electrode. The Tafel plot was derived from the LSV results with a sweep rate of 10 mV/s and a rotating speed of 1600 rpm. RRDE voltammogram was carried out in O_2-presaturated 0.1-M KOH and 0.5-M H_2SO_4 on the disk electrode at a rotating speed of 1600 rpm with a fixed potential of 1.2 V (vs. RHE) in the Pt ring electrode with a scan rate of 10 mV/s, detecting the produced H_2O_2 from the ring electrode. The H_2O_2 selectivity and electron transfer number were estimated from the ring current and disk current at 1600 rpm based on the following equations.[17,18]

$$H_2O_2(\%) = 200 \times \frac{i_{ring}/N}{|i_{disk}| + i_{ring}/N},$$

$$n = \frac{4 \times |i_{disk}|}{|i_{disk}| + i_{ring}/N},$$

where i_{disk} and i_{ring} are the disk and the ring current, respectively, and N is the collection efficiency (N=0.25).

Result and discussion

In this study, we have devised a novel synthetic approach for immobilizing finely dispersed Platinum (Pt) nanoparticles (NPs) by introducing a redox-active covalent organic polymer known as hc-TBtd-COP. The synthetic building unit, TBtd was characterized by ^{1}H-NMR spectroscopy (ESI Fig. S1). The synthesis of hc-TBtd-COP involved the oxidative coupling of TBtd, a Wurster-type functional molecule,[19,20] utilizing ferric chloride as a catalyst,[21] which demonstrated superior efficiency compared to other Lewis acids, like aluminum chloride and tin tetrachloride.

As illustrated in Fig. 1, the preparation of hc-TBtd-COP involved the bridging of two triphenylamine (TPA) units via 2,1,3-Benzothiadiazole core, creating a unique arrangement in the polymerizable monomer. This unique structure enables hc-TBtd-COP to function as a Wurster-type reducing agent for Palladium (II) and Platinum (II). Subsequently, when hc-TBtd-COP was immersed in a Platinum (II) solution, an in situ redox process occurred between the reductive TPA unit and adsorbed Platinum ions. This process led to the confined growth of ultrafine and uniform Pt nanoclusters NCs) inside porous channels.

The presence of TPA units in the TBtd building unit facilitates the confined reduction of Pt inside the pores of hc-TBtd-COP, minimizing the likelihood of reduction occurring in the solution. Moreover, the interaction between Pt NPs and the nitrogen- and sulfur-rich hc-TBtd-COP hinders the spontaneous aggregation of Pt NPs, exposing more active sites. The resulting uniformly confined Pt NPs supported by hc-TBtd-COP make it an efficient electrocatalyst for the oxygen reduction reaction (ORR).

The functional groups of hc-TBtd-COP were characterized by FT-IR spectra. As depicted in Fig. 2(a), characteristic peaks, including the unsaturated stretching (C=C) vibrations at approximately 1485 cm^{-1} and 1591 cm^{-1} and the C–N stretching vibration near 1268 cm^{-1}, were observed for hc-TBtd-COP. These peaks were retained in Pt@hc-TBtd-COP, confirming the existence of the polymerized triphenylamine core.

The materials were characterized using Powder X-ray diffraction (XRD). For pure hc-TBtd-COP, typically no crystalline peak was observed which indicates the amorphous nature of the

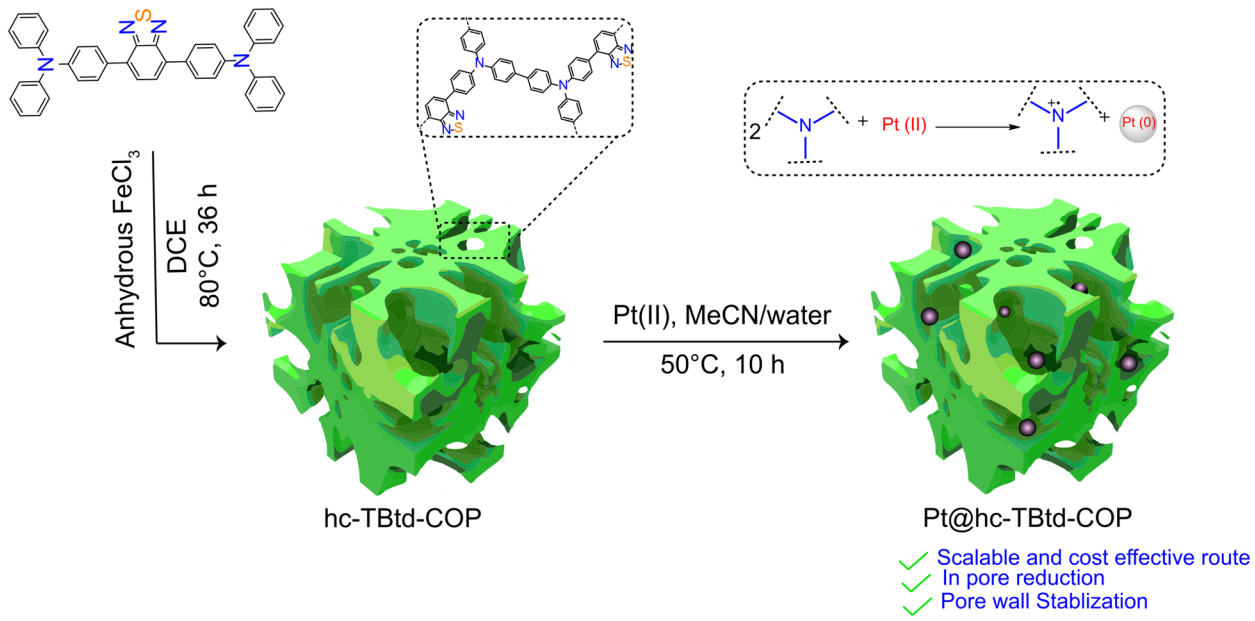

Figure 1. Schematic drawing describing the preparation of Pt@hc-TBtd-COP.

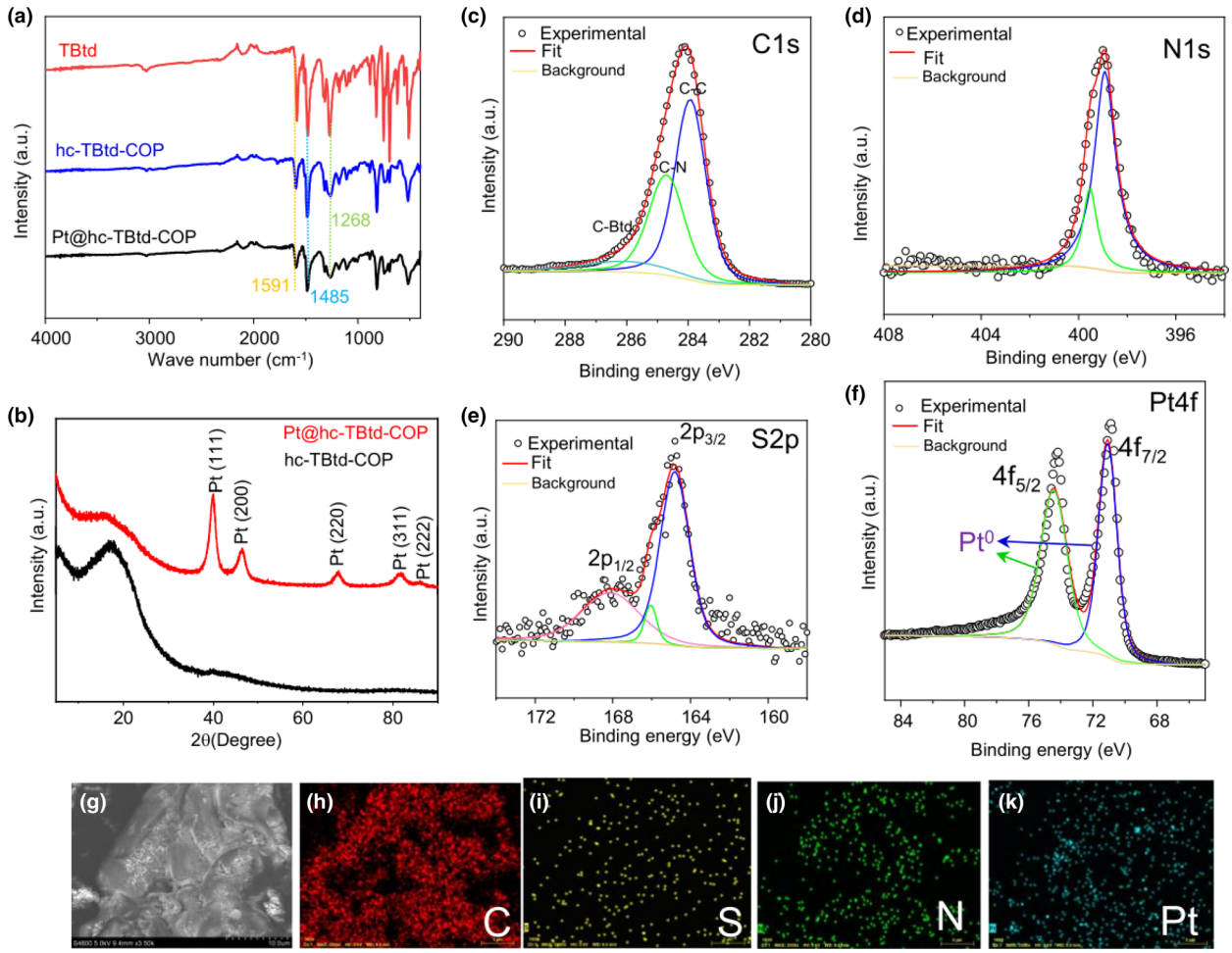

Figure 2. Structural characterizations of Pt@hc-TBtd-COP; (a) Full FT-IR spectra of the TBtd (monomers), hc-TBtd-COP, and Pt@hc-TBtd-COP. (b) Powder X-ray diffraction pattern of hc-TBtd-COP and Pt@hc-TBtd-COP; (c) C1s XPS peak; (d) N1s XPS peak; (e) S2p XPS peak; and (f) Pt4f XPS peak for Pt@hc-TBtd-COP; SEM image of Pt@hc-TBtd-COP and their elemental mapping (g-k, scale bar- 5 μm).

polymer. The PXRD pattern of Pt@hc-TBtd-COP [Fig. 2(b)] displays multiple diffraction peaks, demonstrating the presence of Pt nanoparticles present inside hc-TBtd-COP. The broad hump at 17° corresponds to the amorphous structure of the polymer.[22,23] Meanwhile, PXRD of Pt@hc-TBtd-COP has diffraction peaks between 2θ=40°–90°. The presence of face-centered cubic (fcc) Pt lattice is recognizable, as indicated by the characteristic peaks around 40.05°, 46.64°, 68.02°, 81.95° and 86.27° which can be assigned to the Pt (111), Pt (200), Pt (220), Pt (311), and Pt (311) plane, respectively (JCPDS: 00-004-0802). This indicates the in situ reduction and nucleation of platinum precursor, K_2PtCl_4 to Pt NPs by hc-TBtd-COP. Based on Scherrer's equation (ESI Fig. S2) and the broadening parameter of the Pt (220) peak, the average size of the Pt NP crystallites present inside Pt@hc-TBtd-COP was calculated to be ~3.8 nm.

Pt@hc-TBtd-COP was further investigated by X-ray photoelectron spectroscopy (XPS). A wide range of XPS was recorded to detect the surface composition. Figure 2(c) shows the XPS spectra of the core-level Carbon 1 s electrons. The peak is composed of three subpeaks centered at about 285.9, 284.7, and 283.9 eV which could be assigned for C=N (Btd; 2 1 3-Benzothiadiazole), C–N, and C–C carbons, respectively. Figure 2(d) shows the XPS spectra of core-level N1s electrons. The peak is composed of two subpeaks centered around 398.9, and 399.5 eV which could be assigned for N (triphenylamine) and N (Btd), respectively. S 2p spectra of Pt@hc-TBtd-COP as shown in Fig. 2(e) exhibited three peaks around 164.8, 166.06 eV, and 168.1 eV. Those could be assigned for S2p3/2, S2p1/2, and oxidized sulfur.[22] XPS was conducted to investigate the oxidation state of platinum nanoparticles. The analysis revealed a doublet peak consisting of two Gaussian-shaped components (5/2 and 7/2) with intensity ratios of approximately 3:4. The value of peak separation was approximately ~ 3.3 eV. Platinum 4f electron spectra are shown in Fig. 2(f). The binding energies of Pt 4f7/2 and Pt 4f5/2 were found to be around ~ 71.2 and 74.4 eV, respectively, which demonstrates the presence of

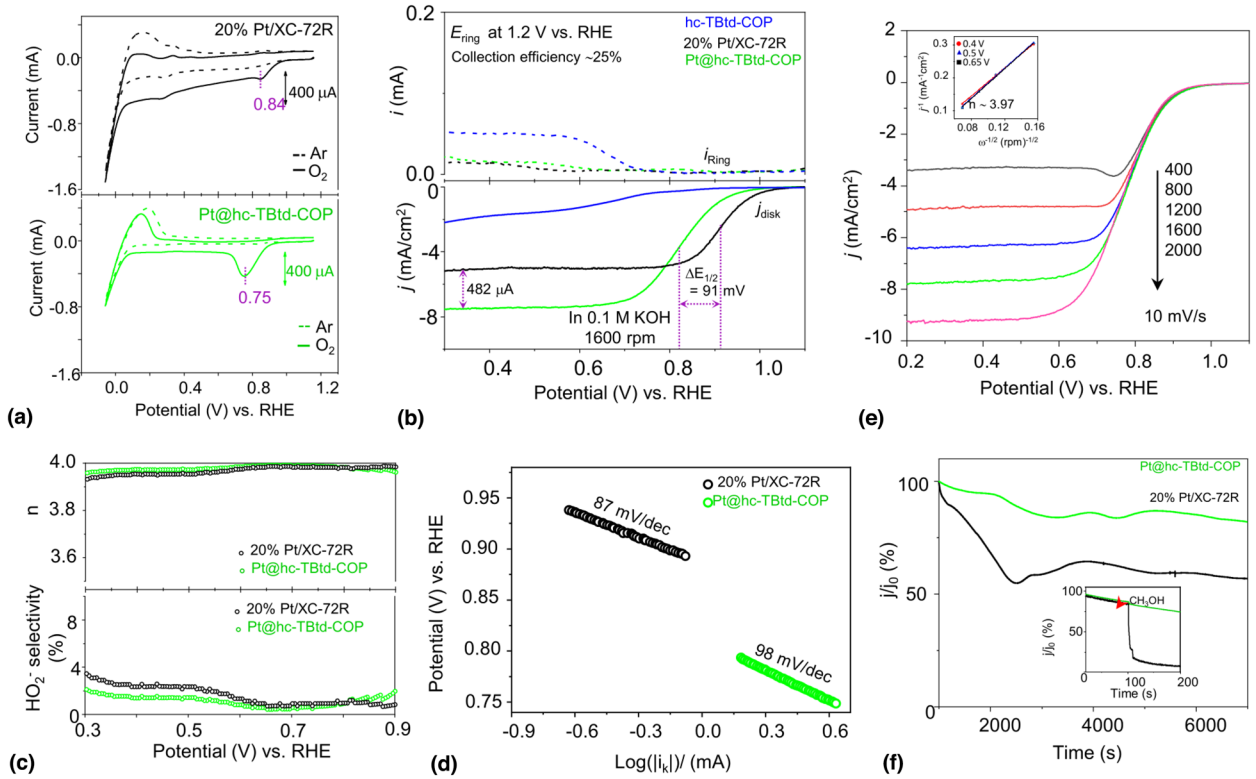

Figure 3. (a) CV curve of Pt@hc-TBtd-COP and commercial 20% Pt/C in 0.1-M KOH at a scan rate of 10 mV/s; (b) The LSV curves of hc-TBtd-COP, Pt@hc-TBtd-COP, and commercial 20% Pt/C were observed using O_2-pre saturated 0.1-M KOH solution at a scan rate of 10 mV/s and a rotation rate of 1600 rpm (rotating ring disk electrode). The detected peroxide currents on the ring electrode were also recorded in the upper panel at a fixed ring potential of 1.2 V vs. RHE; (c) Plot of H_2O_2 selectivity and electron transfer number (n) across ORR potential sweep; (d) Tafel plots; (e) RDE analysis of ORR kinetics of Pt@hc-TBtd-COP with a scan rate of 10 mV s^{-1} at 1600 rpm in O_2-saturated 0.1-M KOH electrolyte (inset: K–L plots at different potentials); and (f) Chronoamperometric stability test for Pt@hc-TBtd-COP and commercial 20% Pt/C obtained in an O_2-saturated 0.1-M KOH (Methanol stability test).

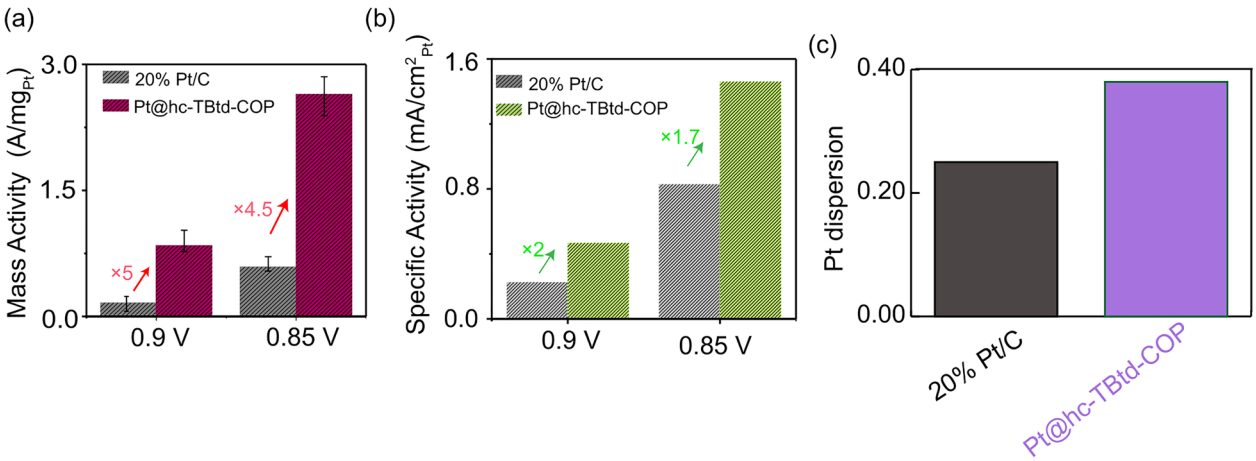

Figure 4. (a) Comparison of mass activity; (b) specific activity; and (c) catalyst dispersion of Pt@hc-TBtd-COP and commercial Pt/C (20%) where potentials are expressed vs. reversible hydrogen electrode.

Pt(0) predominantly in the framework.[24,25] Figure 4(g–k) displays the chemical mapping performed under a scanning electron microscope (SEM) of the elements C, N, S, and Pt which demonstrates the uniform distribution of Pt over the organic matrix.

The catalytic activities of Pt@hc-TBtd-COP were tested in an O_2-presaturated 0.1-M KOH solution. For comparison,

20% Pt/C (XC-72R) (Fuel Cell store, USA) was used. The Cyclic voltammetry curves of Pt@hc-TBtd-COP and the commercial 20% Pt/C catalysts are shown in Fig. 3(a). As shown in Fig. 3(a), Pt@hc-TBtd-COP showed a lower ORR peak observed at 0.75 V with a 361 µA, whereas commercial Pt/C (20%) showed a ~ 90 mV higher ORR reduction peak than that of Pt@hc-TBtd-COP with ORR reduction current around ~ 159 μA. At first, the linear sweep voltammetry (LSV) was performed at 1600 rpm for both catalysts. Figure 3(b) shows the onset potential (Potential to reach the current density − 0.1 mA/cm^2) and half-wave potential ($E_{1/2}$) of Pt@hc-TBtd-COP was found to be slightly lower than commercial Pt/C by 43 mV and 91 mV, respectively. Based on the CV and LSV study, it was observed that Pt@hc-TBtd-COP exhibited ORR activity almost equivalent to that of Pt/C (20%). The Pt@hc-TBtd-COP catalyst has demonstrated nearly identical oxygen reduction reaction (ORR) activity when compared to a 20% commercial Pt/C catalyst. This observation is significant as it addresses the challenge of achieving higher current while utilizing a minimal amount of platinum (Pt). The limiting current (j_L) density was found to be higher for Pt@hc-TBtd-COP than that for Pt/C (20%) by 482 µA which implies that this composite material serves as an excellent ORR electrocatalyst with a higher current density compared to commercial Pt/C (1600 rpm, 10 mV/s). The RRDE experiment was conducted to determine the number of electrons involved in oxygen reduction and the percentage of H_2O_2 production during O_2 electro-reduction in alkaline media for both catalysts. Figure 3(c) illustrates the hydrogen peroxide yield (HO_2^- %) and the number of electrons (n) engaged in the Oxygen Reduction Reaction (ORR) plotted against ORR potential sweeps. These values were derived using disk currents and ring currents. The ring electrode was maintained at a constant potential of 1.2 V vs. RHE to monitor the peroxide oxidation current. For both catalysts (Pt@hc-TBtd-COP and 20% Pt/C), the H_2O_2 yield was determined to be less than 4%. The average number of electrons involved in the process was approximately 3.98. The Tafel plot of Pt@hc-TBtd-COP was also accessed to demonstrate the ORR kinetics which is given in Fig. 3(d). The value of the Tafel slope was determined to be approximately 98 mV dec^{-1}, closely resembling that of a 20% Platinum catalyst. To explore the catalytic activities of the Oxygen Reduction Reaction (ORR) under different rotation rates (400, 800, 1200, 1600, and 2000 rpm), a rotating disk electrode (RDE) experiment was conducted. In Fig. 3(e), the current–potential curves exhibit a dependence on the rotation rate for all the catalysts. Notably, the limiting current density increased with the rotation speed, suggesting that the ORR catalytic process was predominantly governed by oxygen diffusion in all instances. Koutecky–Levich (K–L) plots were scrutinized at various electrode potentials, and the transferred electron number (n) was calculated based on the slopes of these plots [see inset of Fig. 3(e)]. Pt@hc-TBtd-COP demonstrated an average n of approximately 3.97 (at 0.5 V), indicating a 4e- pathway during the ORR. This finding aligns with the outcomes of previous Rotating Ring-Disk Electrode (RRDE) experiments, providing further support for the efficient catalytic performance of Pt@hc-TBtd-COP. In the chronoamperometric I–t study in Fig. 3(f), it was found that Pt@hc-TBtd-COP has a greater stability in current density retention compared to Pt/C catalyst at 0.6 V (vs. RHE) in 0.1-M KOH. Additionally, the methanol tolerance of Pt@hc-TBtd-COP [inset of Fig. 3(f)] was compared with Pt/C to assess its practicality as a methanol-tolerant catalyst.[26] It was observed that upon adding 1 M of methanol, there was no significant change in current density in the case of Pt@hc-TBtd-COP, while Pt/C showed a sudden current density drop under similar conditions which can be attributed to competitive methanol oxidation. The intrinsic ORR activities of Pt@hc-TBtd-COP we estimated by its mass activity, specific activity, and dispersion of the catalyst. Pt@hc-TBtd-COP has delivered the mass activity [Fig. 4(a)] of 0.84 A/mg$_{Pt}$ at 0.9 V and 2.64 A/mg$_{Pt}$ at 0.85 V (vs. RHE), respectively, whereas the MA of commercial Pt/C catalyst was found to be 0.16 A/mg$_{Pt}$ at 0.9 V and 0.58 A/mg$_{Pt}$ at 0.85 V (vs. RHE). Electrochemically active surface area (ECSA) was estimated from the CV of both catalysts in Argon-saturated 0.5-M H_2SO_4 medium (ESI Fig. S(3)). The charge (Q) associated with hydrogen desorption (H_{upd}) between 0 and 0.3 V vs. RHE in CVs and assuming 210 μC/cm^2 charge density required to oxidize a monolayer of H_2 from Pt surface, ECSA was calculated.[27–29] The Q can be determined by integrating the area of the H_{upd} region after double-layer correction. Then, the ECSA is calculated using the following equation:

$$ECSA_{Pt,\left(\frac{m^2}{g_{Pt}}\right)} = \frac{Q_H}{m_{Pt} \times q_H},$$

where Q_H is the charge for H_{upd} adsorption, m is the loading amount of metal, and q_H is the charge (210 μC/cm^2) required for the adsorption of a monolayer of hydrogen on a Pt surface.

ECSA of Pt@hc-TBtd-COP and commercial Pt/C (20%) was found to be 180 m^2/g$_{Pt}$ and 71 m^2/g$_{Pt}$, respectively. Specific activity was calculated by normalizing the kinetic current with ECSA which was found to be 0.467 mA/cm^2 for Pt@hc-TBtd-COP and 0.225 mA/cm^2 for Pt/C at 0.9 V vs. RHE [Fig. 4(b)].[30] The surface average dispersion of Pt in Pt@hc-TBtd-COP was found to be 0.38; whereas, Pt dispersion in Pt/C was found to be 0.25 [Fig. 4(c)].[31]

In conclusion, we have successfully managed to load small-sized platinum nanoparticles into a covalent organic polymer that is rich in nitrogen and sulfur without any external reducing agent. The polymer has pre-designed Wurster-type redox sites that enable the platinum to grow into smaller nanoparticles in a confined environment to give Pt@hc-TBtd-COP. The resulting Pt@hc-TBtd-COP has shown excellent catalytic activity toward alkaline oxygen reduction reaction, compared to commercially available Pt catalysts that have higher loading. This method has dramatically increased the

ECSA values and the mass activity of the Pt. The outstanding catalytic performance of Pt@hc-TBtd-COP can be attributed to the homogeneously distributed smaller Pt nanoparticles on the porous surface of hc-TBtd-COP, which provides a higher exposure of metal-based catalytic sites for ORR. The presence of nitrogen and sulfur creates a charge spin density difference, which boosts the binding strength of neighboring carbon atoms toward oxygen for an enhanced ORR process. This method also dramatically increases the ORR current by providing a favorable channel for enhanced gas diffusion and electrolyte transfer at the electrode interface. This finding not only provides an easy way to generate metal NPs that are uniformly distributed in conjugated organic polymer support, but it also improves the electrochemical performance for oxygen reduction and demonstrates a strategy to achieve higher utilization of catalytic sites for a higher current-to-mass ratio.

Acknowledgments

This work is supported as part of the Center for Alkaline Based Energy Solutions (CABES), an Energy Frontier Research Center funded by the U.S. Department of Energy (DOE), Office of Science, Basic Energy Sciences (BES), under Award # DE-SC0019445. We would also like to acknowledge the financial support from NSF for the acquisition of the XPS equipment (NSF/CHEM 2216473) and the support from the XPS Surface Characterization Facility at the University of Texas at El Paso.

Author contributions

SB and CRC performed the conception and design of this paper. SB and SC performed experiments. All authors read and approved the final manuscript.

Funding

Center for Alkaline Based Energy Solutions (CABES), an Energy Frontier Research Center funded by the U.S. Department of Energy (DOE), Office of Science, Basic Energy Sciences (BES), under Award # DE-SC0019445.

Data availability

The datasets generated during the current study are available from the corresponding author upon reasonable request.

Declarations

Conflict of interest

The authors declare no competing financial interest.

Supplementary Information

The online version contains supplementary material available at https://doi.org/10.1557/s43579-024-00547-2.

References

1. B. Garlyyev, K. Kratzl, M. Rück, J. Michalička, J. Fichtner, J.M. Macak, T. Kratky, S. Günther, M. Cokoja, A.S. Bandarenka, Optimizing the size of platinum nanoparticles for enhanced mass activity in the electrochemical oxygen reduction reaction. Angew. Chem. Int. Ed. **58**, 9596 (2019). https://doi.org/10.1002/anie.201904492
2. M. Eckardt, C. Gebauer, Z. Jusys, M. Wassner, N. Hüsing, R.J. Behm, Oxygen reduction reaction activity and long-term stability of platinum nanoparticles supported on titania and titania-carbon nanotube composites. J. Power. Sources **400**, 580 (2018). https://doi.org/10.1016/j.jpowsour.2018.08.036
3. V. Mastronardi, E. Magliocca, J.S. Gullon, R. Brescia, P.P. Pompa, T.S. Miller, M. Moglianetti, Ultrasmall, coating-free, pyramidal platinum nanoparticles for high stability fuel cell oxygen reduction. ACS Appl. Mater. & Interfaces **14**, 36570 (2022). https://doi.org/10.1021/acsami.2c07738
4. I.H. Hafez, M.R. Berber, T. Fujigaya, N. Nakashima, Enhancement of platinum mass activity on the surface of polymer-wrapped carbon nanotube-based fuel cell electrocatalysts. Sci. Rep. **4**, 6295 (2014). https://doi.org/10.1038/srep06295
5. M. Asahi, S.-I. Yamazaki, N. Taguchi, T. Ioroi, Facile approach to enhance oxygen reduction activity by modification of platinum nanoparticles by melamine-formaldehyde polymer. J. Electrochem. Soc. **166**, F498 (2019). https://doi.org/10.1149/2.0641908jes
6. H. Zhao, G. Yu, M. Yuan, J. Yang, D. Xu, Z. Dong, Ultrafine and highly dispersed platinum nanoparticles confined in a triazinyl-containing porous organic polymer for catalytic applications. Nanoscale **10**, 21466 (2018). https://doi.org/10.1039/C8NR05756G
7. M. Xu, C. Lai, X. Liu, B. Li, M. Zhang, F. Xu, S. Liu, L. Li, L. Qin, H. Yi, COF-confined catalysts: from nanoparticles and nanoclusters to single atoms. J. Mater. Chem. A **9**, 24148 (2021). https://doi.org/10.1039/D1TA04439G
8. L. Liu, A. Corma, Confining isolated atoms and clusters in crystalline porous materials for catalysis. Nat. Rev. Mater. **6**, 244 (2021). https://doi.org/10.1038/s41578-020-00250-3
9. S. Chen, Y. Zheng, B. Zhang, Y. Feng, J. Zhu, J. Xu, C. Zhang, W. Feng, T. Liu, Cobalt, nitrogen-doped porous carbon nanosheet-assembled flowers from metal-coordinated covalent organic polymers for efficient oxygen reduction. ACS Appl. Mater. Interfaces **11**, 1384 (2019). https://doi.org/10.1021/acsami.8b16920
10. S. Bhunia, A. Peña-Duarte, H. Li, H. Li, M.F. Sanad, P. Saha, M.A. Addicoat, K. Sasaki, T.A. Strom, M.J. Yacamán, C.R. Cabrera, R. Seshadri, S. Bhattacharya, J.-L. Brédas, L. Echegoyen, [2,1,3]-Benzothiadiazole-spaced co-porphyrin-based covalent organic frameworks for O_2 reduction. ACS Nano **17**, 3492 (2023). https://doi.org/10.1021/acsnano.2c09838
11. J.-M. Seo, H.-J. Noh, J.-P. Jeon, H. Kim, G.-F. Han, S.K. Kwak, H.Y. Jeong, L. Wang, F. Li, J.-B. Baek, Conductive and ultrastable covalent organic framework/carbon hybrid as an ideal electrocatalytic platform. J. Am. Chem. Soc. **144**, 19973 (2022). https://doi.org/10.1021/jacs.2c08344
12. J. Quinson, A. Dworzak, S.B. Simonsen, L.T. Kuhn, K.M. Jensen, A. Zana, M. Oezaslan, J.J. Kirkensgaard, M. Arenz, Surfactant-free synthesis of size controlled platinum nanoparticles: insights from in situ studies. Appl. Surf. Sci. **549**, 149263 (2021). https://doi.org/10.1016/j.apsusc.2021.149263
13. J. Quinson, J. Mathiesen, J. Schröder, A. Dworzak, F. Bizzotto, A. Zana, S.B. Simonsen, L.T. Kuhn, M. Oezaslan, K.Ø. Jensen, Teaching old precursors new tricks: fast room temperature synthesis of surfactant-free colloidal platinum nanoparticles. J. Colloid Interface Sci. **577**, 319 (2020). https://doi.org/10.1016/j.jcis.2020.05.078
14. M. Peng, C. Dong, R. Gao, D. Xiao, H. Liu, D. Ma, Fully exposed cluster catalyst (FECC): toward rich surface sites and full atom utilization efficiency. ACS Cent. Sci. **7**, 262 (2020). https://doi.org/10.1021/acscentsci.0c01486
15. T. Imaoka, Y. Akanuma, N. Haruta, S. Tsuchiya, K. Ishihara, T. Okayasu, W.-J. Chun, M. Takahashi, K. Yamamoto, Platinum clusters with precise numbers of atoms for preparative-scale catalysis. Nat. Commun. **8**, 688 (2017). https://doi.org/10.1038/s41467-017-00800-4
16. S. Wang, Q. He, C. Wang, H. Jiang, C. Wu, S. Chen, G. Zhang, L. Song, Active Sites engineering toward superior carbon-based oxygen reduction

catalysts via confinement pyrolysis. Small **14**, 1800128 (2018). https://doi.org/10.1002/smll.201800128
17. K. Jiang, S. Back, A.J. Akey, C. Xia, Y. Hu, W. Liang, D. Schaak, E. Stavitski, J.K. Nørskov, S. Siahrostami, Highly selective oxygen reduction to hydrogen peroxide on transition metal single atom coordination. Nat. Commun. **10**, 3997 (2019). https://doi.org/10.1038/s41467-019-11992-2
18. Z. Lu, G. Chen, S. Siahrostami, Z. Chen, K. Liu, J. Xie, L. Liao, T. Wu, D. Lin, Y. Liu, T.F. Jaramillo, J.K. Nørskov, Y. Cui, High-efficiency oxygen reduction to hydrogen peroxide catalysed by oxidized carbon materials. Nat. Catal. **1**, 156 (2018). https://doi.org/10.1038/s41929-017-0017-x
19. W. Wang, L. Zhang, T. Wang, Z. Zhang, X. Wang, C. Cheng, X. Liu, Inner-pore reduction nucleation of palladium nanoparticles in highly conductive wurster-type covalent organic frameworks for efficient oxygen reduction electrocatalysis. J. Energy Chem. **77**, 543 (2023). https://doi.org/10.1016/j.jechem.2022.11.032
20. J.M. Rotter, R. Guntermann, M. Auth, A. Mähringer, A. Sperlich, V. Dyakonov, D.D. Medina, T. Bein, Highly conducting Wurster-type twisted covalent organic frameworks. Chem. Sci. **11**, 12843 (2020). https://doi.org/10.1039/D0SC03909H
21. D. Taylor, S.J. Dalgarno, Z. Xu, F. Vilela, Conjugated porous polymers: incredibly versatile materials with far-reaching applications. Chem. Soc. Rev. **49**, 3981 (2020). https://doi.org/10.1039/C9CS00315K
22. K. Jie, Y. Zhou, Q. Sun, B. Li, R. Zhao, D.-E. Jiang, W. Guo, H. Chen, Z. Yang, F. Huang, S. Dai, Mechanochemical synthesis of pillar[5]quinone derived multi-microporous organic polymers for radioactive organic iodide capture and storage. Nat. Commun. **11**, 1086 (2020). https://doi.org/10.1038/s41467-020-14892-y
23. M.M. Abdelnaby, T.A. Saleh, M. Zeama, M.A. Abdalla, H.M. Ahmed, M.A. Habib, Azo-Linked porous organic polymers for selective carbon dioxide capture and metal ion removal. ACS Omega **7**, 14535 (2022). https://doi.org/10.1021/acsomega.1c05905
24. B. Quan, S.-H. Yu, D.Y. Chung, A. Jin, J.H. Park, Y.-E. Sung, Y. Piao, Single source precursor-based solvothermal synthesis of heteroatom-doped graphene and its energy storage and conversion applications. Sci. Rep. **4**, 5639 (2014). https://doi.org/10.1038/srep05639
25. D. Dang, H. Zou, Z. Xiong, S. Hou, T. Shu, H. Nan, X. Zeng, J. Zeng, S. Liao, High-performance, ultralow platinum membrane electrode assembly fabricated by in situ deposition of a Pt shell layer on carbon-supported Pd nanoparticles in the catalyst layer using a facile pulse electrodeposition approach. ACS Catal. **5**, 4318 (2015). https://doi.org/10.1021/acscatal.5b00030
26. J. Yang, S.H. Kim, S.K. Kwak, H.-K. Song, Curvature-induced metal-support interaction of an islands-by-islands composite of platinum catalyst and carbon nano-onion for durable oxygen reduction. ACS Appl. Mater. Interfaces **9**, 23302 (2017). https://doi.org/10.1021/acsami.7b04410
27. L. Jiao, E. Liu, S. Hwang, S. Mukerjee, Q. Jia, Compressive strain reduces the hydrogen evolution and oxidation reaction activity of platinum in alkaline solution. ACS Catal. **11**, 8165 (2021). https://doi.org/10.1021/acscatal.1c01723
28. T. Xia, J. Liu, S. Wang, C. Wang, Y. Sun, L. Gu, R. Wang, Enhanced catalytic activities of NiPt truncated octahedral nanoparticles toward ethylene glycol oxidation and oxygen reduction in alkaline electrolyte. ACS Appl. Mater. Interfaces **8**, 10841 (2016). https://doi.org/10.1021/acsami.6b01115
29. C.-S. Liu, X.-C. Liu, G.-C. Wang, R.-P. Liang, J.-D. Qiu, Preparation of nitrogen-doped graphene supporting Pt nanoparticles as a catalyst for oxygen reduction and methanol oxidation. J. Electroanal. Chem. **728**, 41 (2014). https://doi.org/10.1016/j.jelechem.2014.06.024
30. W. Chen, Q. Xiang, T. Peng, C. Song, W. Shang, T. Deng, J. Wu, Reconsidering the benchmarking evaluation of catalytic activity in oxygen reduction reaction. iScience (2020). https://doi.org/10.1016/j.isci.2020.101532
31. J. Wang, G. Yin, Y. Shao, Z. Wang, Y. Gao, Platinum deposition on multi-walled carbon nanotubes by ion-exchange method as electrocatalysts for oxygen reduction. J. Electrochem. Soc. **154**, B687 (2007). https://doi.org/10.1149/1.2737343